



SEMI-ACTIVE APPROXIMATION OF RATE-INDEPENDENT LINEAR DAMPING FOR THE SEISMIC PROTECTION OF LOW-FREQUENCY STRUCTURES

A. Keivan⁽¹⁾, B.M. Phillips⁽²⁾, M. Ikenaga⁽³⁾, K. Ikago⁽⁴⁾

⁽¹⁾ Ph.D. Candidate, Department of Civil and Environmental Engineering, University of Maryland, College Park, United States, akeivan1@umd.edu

⁽²⁾ Assistant Professor, Department of Civil and Environmental Engineering, University of Maryland, College Park, United States, bphilli@umd.edu

⁽³⁾ Associate Professor, Department of Architecture, Faculty of Environmental and Urban Engineering, Kansai University, Osaka, Japan, mikenaga@kansai-u.ac.jp

⁽⁴⁾ Professor, Department of Architecture and Building Science, Tohoku University, Sendai, Japan, ikago@archi.tohoku.ac.jp

Abstract

Rate-independent linear damping, also known as linear hysteretic damping or complex-value stiffness, provides direct control over displacement, a desirable feature for low-frequency structures. The greatest benefit is realized when the frequency of the input is larger than the frequency of the structure, typical of low-frequency structures under earthquake excitations. In such scenarios, rate-independent linear damping provides comparable reduction in displacement and velocity as other damping types with greater acceleration reduction and at about half of the restoring force. In rate-independent linear damping, the restoring force is proportional to displacement but in phase with velocity, leading to its non-causality. Numerical investigations have illustrated the promise of rate-independent linear damping through non-causal time-domain and frequency-domain analyses. However, there are limited practical approaches to determine the rate-independent force through causal analysis. Causal determination of the force associated with rate-independent linear damping will facilitate the realization of this force through semi-active or active control methods. This study proposes a filter-based approach to approximate rate-independent linear damping. The filter is used to approximate the preceded displacement, which is by definition proportional to the desired force. A semi-active control algorithm is then used to track the desired force. The approach is demonstrated for a hybrid base-isolation system with a magnetorheological damper incorporated in isolation layer of a base-isolated structure. Both numerical and experimental tests are conducted to examine the performance of this method to achieve the ideal damping force. Results compare very well with non-causal numerical simulations, confirming both through simulation and experimentation the proposed approach to achieve the benefits of rate-independent linear damping in practical structures.

Keywords: rate-independent linear damping; base isolation; structural control

1. Introduction

The recent 2011 Tohoku Earthquake produced devastating low-frequency ground motions which led to large displacements in low-frequency structures previously thought to be safe, including base-isolated structures ([1] - [2]). Base-isolated structures are particularly vulnerable because large displacements at the isolator layer can cause permanent damage to the isolators or the surrounding moat wall. Base isolation is often supplemented with viscous or hysteretic damping devices at the isolation layer (i.e., hybrid isolation, see Fig. 1) to reduce these displacements. However, the performance of these systems can be compromised by low-frequency ground motions. Low-frequency ground motions are low velocity, leading to poor performance for viscous damping systems. Low-frequency ground motions also produce large displacements, leading to a low equivalent damping ratio for hysteretic damping systems. Fig. 2 provides a qualitative illustration of this behavior. Straightforward solutions such as adding more dampers will compromise the system performance under high-frequency ground motions, amplifying damping forces and structural accelerations [3]. Improvements to hybrid systems must be tempered with the likelihood that high-frequency ground motions can still occur.

Rate-independent linear damping, also known as linear hysteretic damping, complex-value stiffness, structural damping, and solid damping ([4] - [6]) provides an attractive control alternative for low-frequency structures by providing direct control over displacement. The greatest benefit is realized when the excitation frequency is larger than the frequency of the structure, typical of low-frequency structures under earthquake excitations. In such scenarios, rate-independent linear damping provides a comparable reduction in displacement and velocity as other damping types with greater acceleration reduction and at about half of the restoring force [3]. In rate-independent linear damping, the restoring force is proportional to displacement advanced in phase by $\pi/2$ radians (90°), leading to its non-causality.



Fig. 1 – Hybrid base-isolation system on the campus of Tohoku University.

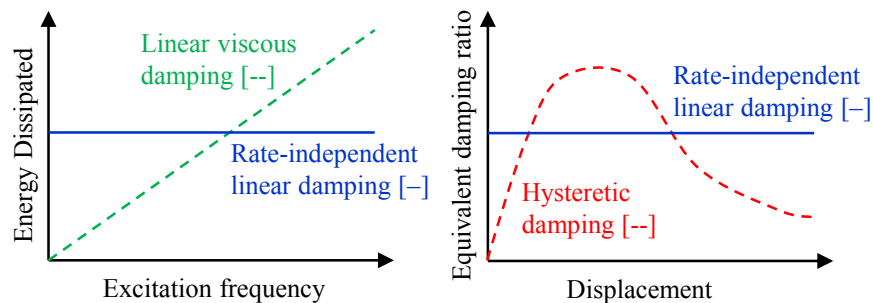


Fig. 2 – Rate-independent linear damping versus other damping types.

A viscoelastic model for rate-independent linear damping was first presented by Biot [8]. This model consists of a linear spring in parallel with a large number of Maxwell elements (spring-dashpot links). Crandall [9] first proposed that ideal rate-independent damping is non-causal. Crandall [10] further investigated the performance of different damping devices using transfer functions in frequency domain and impulse response function in time domain and concluded that a damper with frequency independent energy dissipation per cycle (see Fig. 2) violates causality requirements. In another study, Makris [11] created and analyzed a causal hysteretic element that generates frequency independent energy dissipation. In Makris [11], an adjustable term is added to ideal rate-independent linear damping to satisfy causality. The performance of their proposed model



was shown to be a limiting case of the linear viscoelastic model that was proposed by Biot [8]. The protection of low-frequency structures stands to benefit from causal realizations of rate-independent linear damping. This paper proposes a new simple causal realization accompanied by experimental results to validate the beneficial performance.

This paper addresses the challenges of representing non-causal damping with causal systems for practical engineering applications. This paper explores the theoretical development and behavior of rate-independent linear damping to inform causal implementations. A simple filter based approach is proposed to approximate the ideal rate-independent damping force in real time. The force is then tracked by a control device, selected as an MR damper for this study. Because rate-independent linear damping is in phase with velocity, semi-active dampers such as MR dampers are well-suited for this application. Both numerical simulations and shake table tests are conducted to examine the efficiency of this method in practical applications.

2. Non-causal Analysis

Structures employing rate-independent linear damping require knowledge of the entire time history of the input due to their non-causality [12]. Two methods are commonly used for the analysis of these systems: non-causal time domain analysis and frequency domain analysis. Inaudi and Kelly [13] and Inaudi and Makris [14] propose non-causal time domain approaches in which they show that the true frequency domain and time domain representation of rate-independent linear damping are as follows:

$$F_D(\omega) = \eta k i \text{sign}(\omega) X(\omega) \quad (1)$$

$$f_D(t) = k \eta \hat{x}(t) \quad (2)$$

where $\hat{x}(t)$ is Hilbert transform of $x(t)$.

Eq. (2) provides insight into the behavior of rate-independent linear damping and its relationship with the Hilbert transform, however, it is clear that causal methods are needed to approximate the ideal damping force for practical implementation.

2.1 Non-causal Frequency domain analysis

Time domain techniques provide insight into rate-independent linear damping to inform causal implementations. However, frequency domain analysis is the most straightforward method to handle a linear non-causal system [15]. Combining mass, viscous damping, rate-independent linear damping, stiffness, and ground motion into one SDOF system results in the following general equation of motion:

$$m\ddot{x}(t) + c\dot{x}(t) + k\eta\hat{x}(t) + kx(t) = -m\ddot{x}_g(t) \quad (3)$$

Taking the Fourier transform of both sides of the Eq. (3) results in:

$$\left(-m\omega^2 + ci\omega + k\eta i \text{sign}(\omega) + k\right) X(\omega) = -m\ddot{X}_g(\omega) \quad (4)$$

Based on Eq. (4), the displacement transfer function can be computed as follows:

$$H_d(\omega) = \frac{-m}{-m\omega^2 + ci\omega + k\eta i \text{sign}(\omega) + k} \quad (5)$$

Velocity and acceleration transfer functions can be calculated from the displacement transfer function. The time domain response displacement can be calculated using the inverse Fourier transform as follows:



$$x(t) = \mathfrak{F}^{-1} \left[H_d(\omega) \ddot{X}_g(\omega) \right] \quad (6)$$

Note that the frequency domain response must be calculated separately for positive and negative frequencies to accommodate the *sign* function of Eq. (5). The responses must then be appended to include the response over the entire frequency range before taking the inverse Fourier transform. This method is applicable for MDOF structures if the m , c , k , and η are replaced with corresponding matrices and the ground motion acceleration input is distributed to the appropriate masses. For its simplicity, the frequency domain approach is used in the remainder of this paper.

2.2 Historic ground motions

Three well-studied earthquake ground motion records with different magnitudes and frequency content are selected for analysis in this study [16]: (1) Hachinohe: The N-S component recorded at Hachinohe Harbor during the Tokachi-oki earthquake of May 16, 1968, (2) Northridge: the N-S component of the Sylmar County Hospital parking lot in Sylmar, California during the Northridge earthquake of January 17, 1994, and (3) Kobe: the N-S component of the Japanese Meteorological Agency station during the Kobe earthquake of January 17, 1995. The reference earthquakes are passed through a 2-pole Butterworth high-pass filter with a cutoff frequency of 0.25 Hz. This pre-filtering removes the low-frequency behavior without altering the desired frequency content to avoid significant shake table drift in the experimental studies.

3. Proposed Causal Realization

To realize the benefits of direct displacement control for low-frequency structures, an accurate causal realization of rate-independent linear damping is needed. Eq. (1) correctly represents the rate-independent linear damping force in the frequency domain. The force can be broken into two components, the constant $k\eta$ and the transfer function:

$$H_{TF}(\omega) = i \text{sign}(\omega) \quad (7)$$

Passing the response displacement for a particular device through the transfer function of Eq. (7) and then multiplying by $k\eta$ will produce the rate-independent linear damping force. Thus, Eq. (7) is taken as the target filter for causal realization. The target filter has unity magnitude and phase advance of $\pi/2$ rad over all positive frequencies. The target filter cannot be implemented in a causal system; however, it can be approximated over a specified frequency range using a first-order all-pass filter:

$$H_{AP}(\omega) = \frac{i\omega - \alpha}{i\omega + \alpha} \quad (8)$$

where α is a filter design parameter. Most structures will predominately respond at their first natural frequency. Therefore, the all-pass filter should best match the target filter at the first natural frequency of the structure. The phase of $H_{AP}(\omega)$ is calculated as:

$$\varphi(\omega) = \pi - 2 \tan^{-1} \left(\frac{\omega}{\alpha} \right) \quad (9)$$

Setting $\varphi(\omega_n) = \pi/2$ rad in Eq. (9) (the desired phase at the desired frequency), results in parameter α is equal to ω_n . Therefore, the all-pass filter will take the form:

$$H_{AP}(\omega) = \frac{i\omega - \omega_n}{i\omega + \omega_n} \quad (10)$$

Fig. 3 compares the magnitude and phase of the target filter with the first-order all-pass filter. At and around the natural frequency of the structure, the proposed filter design matches the phase of the target filter. At all frequencies, the proposed filter design matches the magnitude of the target filter.

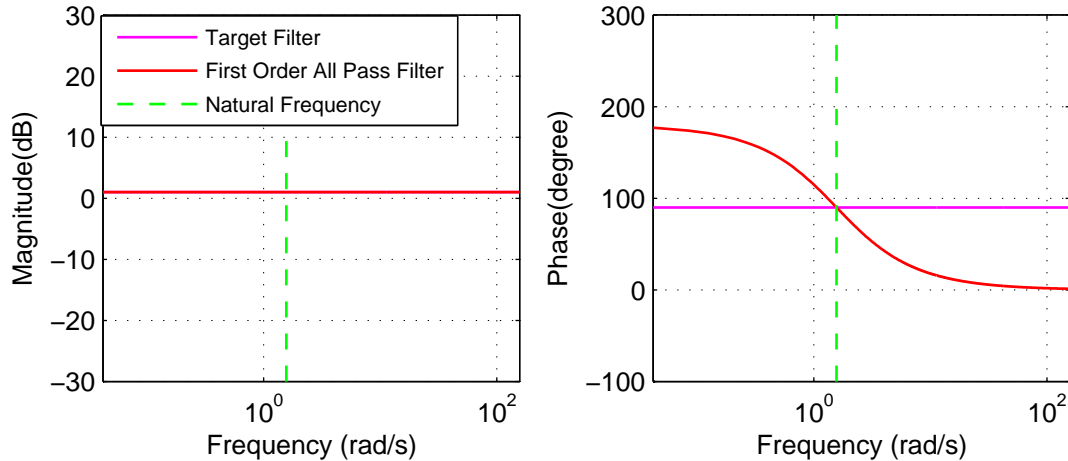


Fig. 3– Magnitude and phase of the target and all-pass filters.

Passing a displacement through the target filter is equivalent to taking its Hilbert transform, a necessary step in the time domain realization of rate-independent linear damping. Since this filter cannot be implemented, an all-pass filter is proposed to approximate the Hilbert transform at the natural frequency of the structure. This approach is applicable to SDOF systems as well as MDOF systems where the filter can be tuned to the first natural frequency of the structure. Base-isolated systems are heavily dominated by first mode response, making this approach particularly attractive.

The proposed filter is used to determine the preceded displacement in a causal manner. The preceded displacement is then multiplied by $k\eta$ to determine the corresponding rate-independent linear damping force. The only measurement needed to implement this method is the displacement of the device. For example, the displacement of the base-isolation layer can be used to determine the corresponding rate-independent linear damping force in a hybrid isolation system. The force can then be tracked by an active or semi-active control device. This simplicity is a great benefit for practical implementation.

4. Experimental Setup

Experimental studies are needed to ensure that the desired calculated forces can be physically and practically realized. Shake table testing offers a simple means to experimentally evaluate the performance of a structure subject to a ground motion. Tohoku University has a 3m × 3m bi-directional shake table and a steel frame specimen that is well-suited for this study. The structure of interest is a base-isolated specimen with supplemental damping at the isolation layer. Through the proposed algorithm, the supplemental damper will behave as a rate-independent linear damping device.

4.1 Base-isolated specimen

The specimen is a single-story structure mounted on an isolation system. The isolation system consists of four linear bearing blocks that can slide on two linear guide rails with very low friction and four steel coil springs to provide restoring forces. The stiffness of the isolated specimen is 12.3 kN/m. Steel weights are mounted on the top and the base of the specimen. The roof mass including the mass of the steel frame members is 2.08 metric tons, and the base mass including the mass of the steel base frame is 2.92 metric tons. When the braces of the specimen are locked, the specimen acts as an SDOF system with a mass of 5 tons and natural frequency of 0.25 Hz. Fig. 4 shows an image of the base isolated specimen with braces locked.



Fig. 4 – Base-isolated specimen with braces locked.

4.2 MR damper specimen

Semi-active devices provide a straightforward means to physically deliver rate-intendent linear damping. MR dampers are well-studied semi-active devices and an excellent alternative for this application. The response of the damper is naturally in phase with the velocity of response and the magnitude of the response can be adjusted online through a control algorithm. The unique properties of MR dampers are derived from the internal MR fluid. In the presence of a magnetic field, the fluid changes from a linear viscous fluid to a semi-solid with controllable yield strength [17]. The source of the magnetic field is an electromagnet, excited by an external current which can vary as required by a control algorithm.

To achieve causal desired rate-independent linear damping, a long stroke MR damper is placed at the isolation level. A schematic of the long stroke damper is shown in Fig. 5. The length of the damper in neutral position is 2,305 mm and the stroke is ± 400 mm.

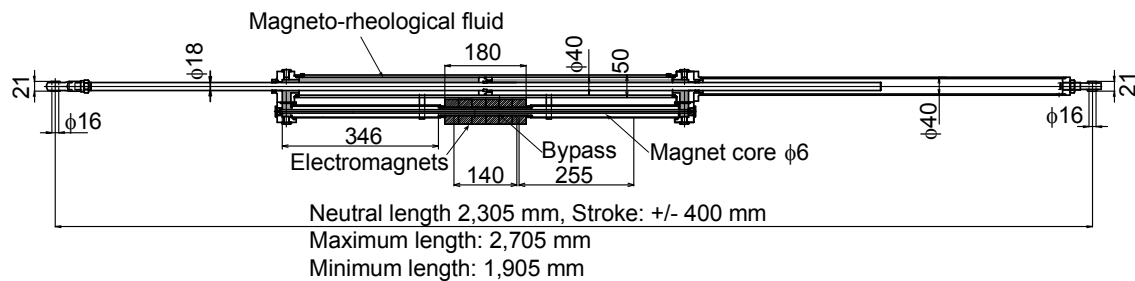


Fig. 5 – Long-stroke MR damper.

The proposed all-pass filter is designed through selection of η to produce a desired force within the range of forces achievable by the MR damper. Many semi-active control algorithms are available to track a desired force using an MR damper. For this application, a feedforward control algorithm was developed. Based on sine wave characterization tests, an approximate relationship was developed between the damping force and input voltage:

$$f_{MR} = 0.1V^2 + 72V + 46.4 \quad (11)$$

where f_{MR} is the damping force in kN and V is the input voltage in Volts. Solving for the input voltage V required to achieve a desired force, the equation can be rewritten as:

$$V = 5\sqrt{400|f_{MR}| + 32.28} - 36 \quad (12)$$

Eq. (12) determines the command voltage for the MR damper based on the desired damping force. In this controller, if the measured and desired force have the same sign, the input voltage to the MR damper is computed using Eq. (12); however, if they have opposite signs, the input voltage to the MR damper is set to zero. Fig. 6 shows an experimental example of the tracking of the desired force by the measured force using this algorithm. The results are for an SDOF system with mass of 5 metric tons, natural frequency of 0.25 Hz, loss factor η of 0.6, and no viscous damping subjected to 50% Hachinohe earthquake ground motion. The desired force is determined using the proposed all-pass filter. It is worth mentioning that the passive-off (0 V) limitation of the damper is about 0.1 kN; therefore, the damper force cannot generally decrease beyond that limit except under very small velocities.

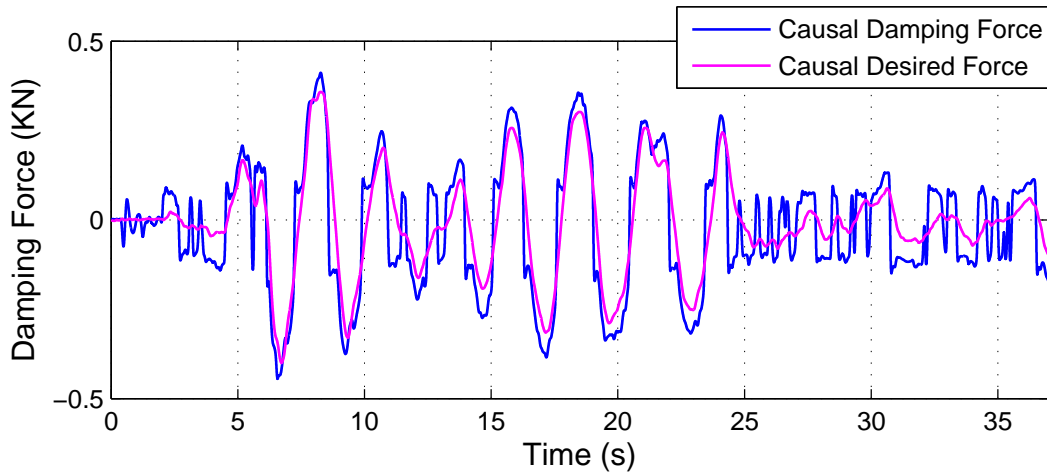


Fig. 6 – Desired and measured damping force using the force tracking control algorithm.

5. Experimental Results and Discussion

A series of shake table tests were conducted at Tohoku University to examine the performance of the proposed causal realization of rate-independent linear damping. Load cells, accelerometers, and displacement transducers were used to capture damping force, acceleration, and displacement system respectively. In the experiments, the specimen is the base-isolated specimen with MR damper installed in the isolation layer described in Section 4. The loss factor η may be freely selected, influencing the magnitude of the rate-independent linear damping to be tracked by the MR damper. The desired force should fall within the MR damper's controllable range; otherwise the MR damper design is not suited for the application. Unless otherwise noted, η is selected as 0.6. The non-causal analyses are performed in the frequency domain using identified structural parameters and an ideal rate-independent linear damper in place of the MR damper.

5.1 Comparisons of causal and non-causal approaches

In this section, the ability of the proposed causal approach to achieve rate-independent linear damping is evaluated. Results are compared to ideal rate-independent linear damping determined through a frequency domain analysis. Fig. 7 illustrates displacement, absolute acceleration, and damping force time histories in both experiment (causal) and frequency domain (non-causal) when the structure is subject to the Hachinohe earthquake with 50% intensity. Fig. 7 also includes the MR damper hysteresis in comparison to non-causal hysteresis from frequency domain analysis.

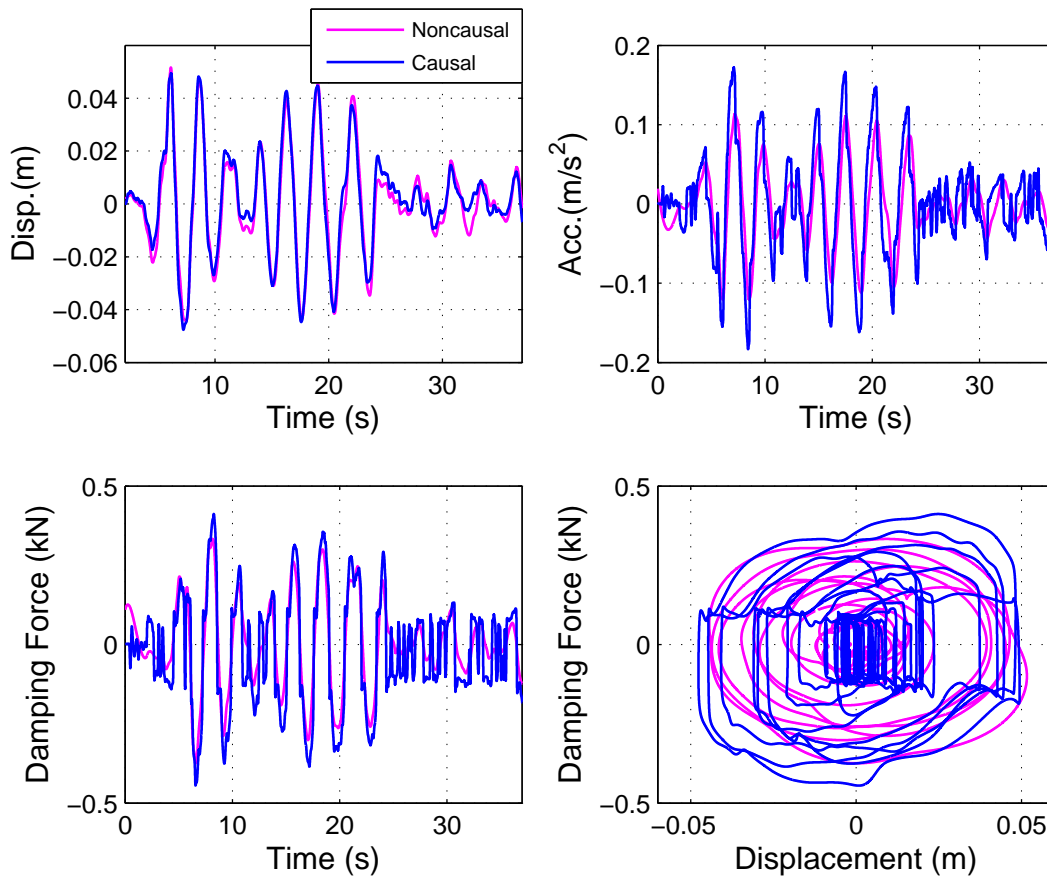


Fig. 7 – Causal and non-causal displacement, absolute acceleration, damping force, and hysteresis for 50% Hachinohe earthquake.

As it is shown in Fig. 7, the experimental causal displacement has a very good match with non-causal displacement from frequency domain analysis. However, the experimental acceleration has larger peaks than those of the frequency domain analysis. This is due to an inability to exactly reproduce the reduced acceleration of true rate-independent linear damping. Fig. 7 also depicts the experimental causal damping force recorded during the experiment as compared to the analytical non-causal damping force. There is a very good agreement in both time history and hysteresis, illustrating that both the calculation of the desired causal force and tracking of the desired causal force using the MR damper perform very well.

To illustrate the proposed algorithm performance under an earthquake with different frequency content, 30% intensity of the Kobe earthquake was applied to the structure in both experiment and numerical analysis. Fig. 8 shows the displacement, absolute acceleration, damping force, and force hysteresis of the experimental tests compared with the same quantities from a non-causal analysis.

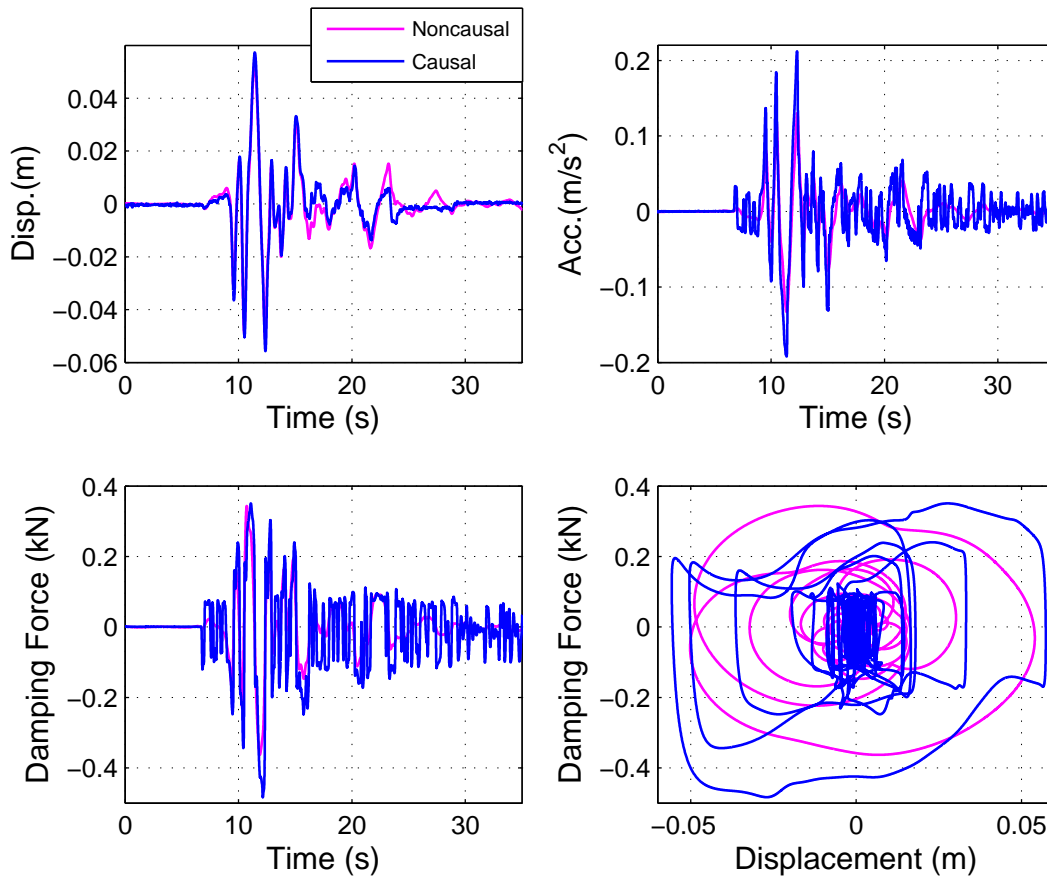


Fig. 8 – Causal and non-causal displacement, absolute acceleration, damping force, and hysteresis for 30% Kobe earthquake.

For the case of the Kobe earthquake, again there is a good match between non-causal simulation and experiments for the displacement time history and the damping force time history as is shown in Fig. 8. There is a larger difference between the experimental acceleration and non-causal acceleration when compared to the same two parameters under the Hachinohe earthquake. Additionally, the hysteresis loop of the experimental force under the Kobe earthquake is more skewed. The Kobe earthquake caused the structure to respond at both its natural frequency and with a forced vibration of about twice its natural frequency. Using the proposed filter-based method, response at a frequency larger than the natural frequency of the structure will introduce a phase lag to the desired force. This produces a skewed force hysteresis and larger acceleration response. Aside from a slightly degraded performance, the proposed approach works well even when the response drifts away from the natural frequency of the structure.

The Kobe earthquake represents a special case. To illustrate the benefits and generality of this method, a third example is introduced. The Northridge earthquake with 30% intensity is applied to the structure in both experiment and analysis. Fig. 9 depicts experimental responses versus non-causal numerical analysis results for this earthquake.

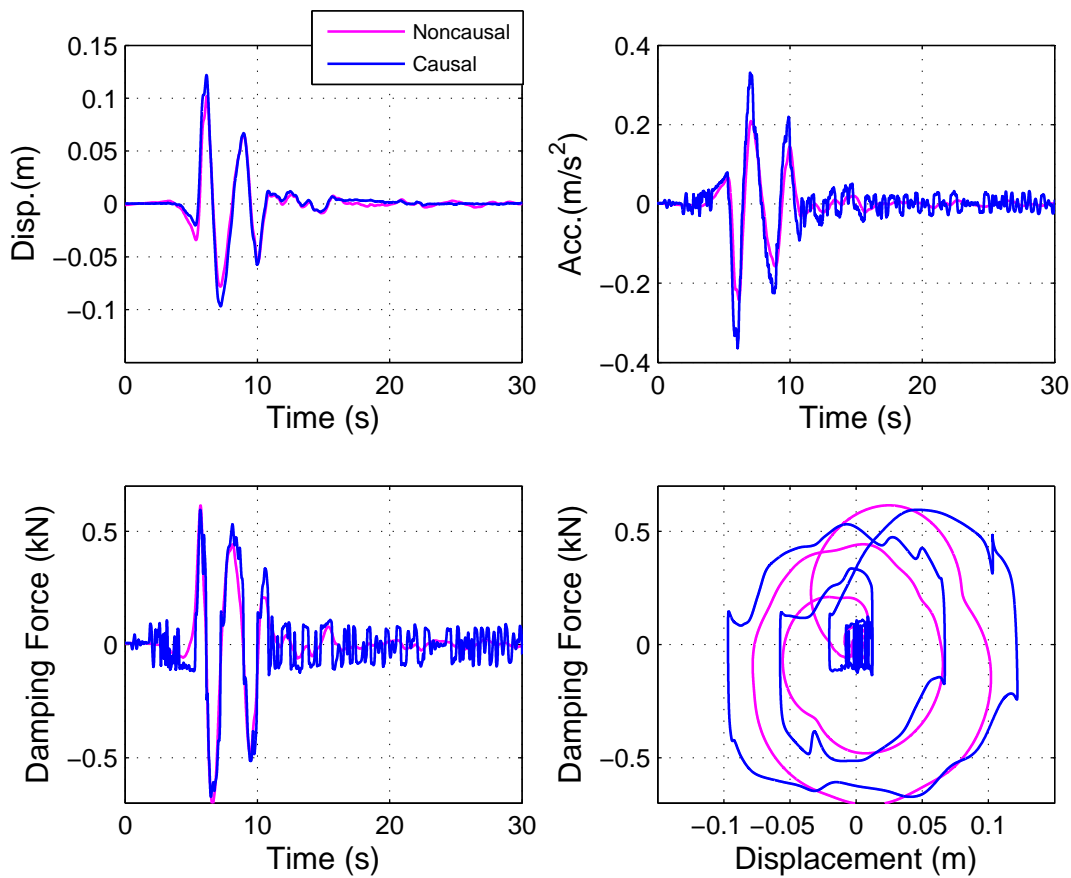


Fig. 9 – Causal and non-causal displacement, absolute acceleration, damping force, and hysteresis for 30% Northridge earthquake.

Under the Northridge earthquake, the causal linear rate-independent damping force is very close to non-causal damping force and there is a match between causal and non-causal hysteresis. In studying the three earthquakes with very different frequency content, the robustness of the proposed causal realization of rate-independent linear damping has been demonstrated.

6. Conclusion

This paper presents a causal method to achieve rate-independent linear damping for the protection of low-frequency structures. In this method, an all-pass filter is designed with constant magnitude and a $\pi/2$ rad phase advance at a prescribed frequency, selected as the first natural frequency of the structure. The device-level response displacement of the structure is passed through the filter to determine the preceded displacement, approximating the Hilbert transform. Therefore, the only measurement needed is the displacement of the device. For example in hybrid isolation, the displacement at the isolation level can be used to determine the desired force to be tracked by a semi active (or active) device. This simplicity and need for only local sensors is a great benefit for practical implementation.

Numerical analyses and experimental tests with different input ground motions were conducted to demonstrate the robustness and applicability of this method across a broad range of inputs. Experimental tests used an MR damper at the isolation layer of a base-isolation system. This desired force was computed at each time step from the preceded displacement. A feedforward control algorithm was employed to track the desired force with the MR damper. For comparison, a frequency domain approach was used to determine the non-causal response of the structure an ideal rate-independent linear device in place of the MR damper.



Experimental results were shown to accurately reproduce non-causal analysis, achieving rate-independent linear damping behavior for multiple input ground motions. The proposed controller was shown to require one sensor, no iteration on design, and a meaningful and achievable desired force. The proposed controller can also be readily applied in active control systems due to its robust design and smooth and stabilizing control force.

Overall, the proposed controller is able to achieve damping with direct displacement control, a great benefit for limiting the displacement response of low-frequency structures through low control forces (and thus low accelerations) when compared to traditional approaches.

7. Acknowledgements

This material is based upon work supported by the National Science Foundation under Grant No. 1444160 and by the Japan Society for the Promotion of Science (JSPS) under Grant-in-Aid for Scientific Research (B) No. 15H04070. Any opinions, findings, and conclusions or recommendations expressed in this material are those of the authors and do not necessarily reflect the views of these agencies.

8. References

- [1] Mimura N, Yasuhara K, Kawagoe S, Yokoki H, Kazama S (2011): Damage from the Great East Japan Earthquake and Tsunami: a quick report. *Mitigation and Adaptation Strategies for Global Change*, **16**(7), 803-818.
- [2] Takewaki I, Murakami S, Fujita K, Yoshitomi S, Tsuji M (2011): The 2011 off the Pacific coast of Tohoku earthquake and response of high-rise buildings under long-period ground motions. *Soil Dynamics and Earthquake Engineering*, **31**(11), 1511-1528.
- [3] Ikago K, Inoue N. Behavior of Rate-independent Linear Damping Incorporated into Long-period Structures Subjected to Strong Ground Motions. *Proceeding of 6th World Conference on Structural Control and Monitoring*. Barcelona, Spain 2014; Paper 273.
- [4] Bishop RED (1955): The treatment of damping forces in vibration theory. *Journal of Royal Aeronautical Society*, **59**, 738-742.
- [5] Reid TJ (1956): Free vibration and hysteretic damping. *Journal of Royal Aeronautical Society*, **60**(283).
- [6] Lancaster P (1960): Free vibration and hysteretic damping. *Journal of Royal Aeronautical Society*, **64**(229).
- [7] Caughey T.K, Vijayaraghavan (1970): Free and forced oscillations of a dynamic system with linear hysteretic damping (non-linear theory). *International Journal of Non-Linear Mechanics*, **5**(3), 533-555.
- [8] Biot M.A (1958): Linear Thermodynamics and the Mechanics of Solids. *Proceedings of the 3rd U.S. National Congress of Applied Mechanics (ASME)*, New York, N.Y. 1958; 1-18.
- [9] Crandall SH (1963): Dynamic response of systems with structural damping. *Air space and instruments*. McGraw-Hill Book Company, inc, 183.
- [10] Crandall SH (1991): The Hysteretic Damping Model in Vibration Theory. *Journal of Mechanical Engineering Science, Proceedings of the institution of Mechanical Engineering*, 205C, 23-28.
- [11] Makris N (1997): The causal hysteretic element, ASCE. *Journal of Engineering Mechanics*, **123**(11), 1209-1214.
- [12] Crandall SH (1963): Dynamic response of systems with structural damping. *Air space and instruments*. McGraw-Hill Book Company, inc, 183.
- [13] Inaudi JA, Kelly JM (1995): Linear Hysteretic Damping and the Hilbert Transform. *Journal of Engineering Mechanics*, **121**(5), 0626-0632.
- [14] Inaudi JA, Makris N (1996): Time Domain Analysis of Linear Hysteretic Damping. *Earthquake Engineering and Structural Dynamics*, **25**(6), 529-545.
- [15] Nashif T.J, Jones I.G, Henderson J.P (1988): *Vibration damping*. Wiley, New York.
- [16] Ohtori Y, Christenson RE, Spencer BF Jr, Dyke SJ (2004): Benchmark control problems for seismically excited nonlinear buildings. *Journal of Engineering Mechanics*, **130**(4), 366-385.
- [17] Carlson JD, Jolly MR (2000): MR fluid, foam, and elastomer devices. *Mechatronics*, **10**(4-5), 555-569.